OMAE-22-1166

Influence on structural loading of a wave energy converter by controlling variable-geometry components and the power take-off

Salman Husain[1], **Jacob Davis**[2], **Nathan Tom**[1], **Krish Thiagarajan**[2]

Cole Burge[3], **Nhu Nguyen**[2‡]

ABSTRACT

Oceans are harsh environments and can impose significant loads on deployed structures. A Wave Energy Converter (WEC) should be designed to maximize the energy absorbed while ensuring the operating wave condition does not exceed the failure limits of the device itself. Therefore, the loads endured by the support structure are a design constraint for the system. Furthermore, the WEC should be adaptable to different sea states. This work uses a WEC-Sim model of a variable-geometry oscillating wave energy converter (VGOSWEC) mounted on a support structure simulated under different wave scenarios. A VGOSWEC resembles a paddle pitching about a fixed hinge perpendicular to the incoming wave fronts. The geometry of the VGOSWEC is varied by opening a series of controllable flaps on the pitching paddle when the structure experiences threshold loads. It is hypothesized that opening the flaps should result in load shedding at the base of the support structure by reducing the moments about the hinge axis. This work compares the hydrodynamic coefficients, natural periods, and response amplitude operators from completely closed to completely open configurations of the controllable flaps. This work shows that the completely open configuration can reduce the pitch and surge loads on the base of the support structure by as much as 80%. Increased loads at the structure's natural period can be mitigated by an axial power take-off damping acting as an additional design parameter to control the loads at the WEC's support structure.

[*1]Salman Husain and Nathan Tom are with the Water Power Department, National Renewable Energy Laboratory, Golden, CO 80401, USA sal.husain@nrel.gov,nathan.tom@nrel.gov

[†2]Jacob Davis, Krish Thiagarajan Sharman, and Nhu Nguyen are with the Department of Mechanical and Industrial Engineering, University of Massachusetts Amherst, Amherst, MA 01003, USA jacrdavis@umass.edu, kthiagarajan@umass.edu, nvnguyen@umass.edu

[‡3]Cole Burge is with the Department of Mechanical Engineering, University of Washington, Seattle, WA 98195, USA coleburge@gmail.com

1 INTRODUCTION

In recent years renewable energy devices have achieved design convergence for solar and wind, but the research community designing marine energy extraction devices is still exploring various wave energy converters (WECs). WEC designs range from devices that are axisymmetric - usually oscillating in heave, and asymmetric - usually oscillating in surge or pitch modes [1]. An axisymmetric WEC (e.g., the CorPower WEC [2]) is agnostic to the incoming wave direction but sacrifices a significant amount of energy that could otherwise be extracted in modes that are orthogonal to the primary oscillating mode of the incoming wave, as discussed by Korde et al. in their discussion on terminator-type WECs [1].

Terminator-type WECs extract energy from motion orthogonal to the mean incoming wave spectra.Some notable examples of WECs in terminator configuration include Salter's Duck, which extracts energy using the mode-coupling of its surge, heave, and pitch modes, the Oyster WEC which extracts wave energy from its pitch modeand the free-floating sloped Interproject Service (IPS) buoy, which extracts energy by the mode-coupling of its surge and heave modes [3–7]. Water particles in typical oceanic waves move in elliptical trajectories, and as they approach the coast these elliptical trajectories flatten out such that a significant amount of wave energy propagates in the surge mode and the rotational mode orthogonal to the propagating wave, i.e., the pitch mode [8–10].Terminator-type devices are usually suitable for near-shore deployment because they extractenergy of the water particles in the horizontal direction. The near-shore deployment of terminator-type WECs opens up the possibility of rigid support structures that can allow greater motion in the power take-offs (PTOs) and generate greater power compared to devices like the Reference Model 5 or the Langlee WEC [11].

Li and Yu, reviewed the numerical methods used for modeling WECs, identifying four major approaches; (i.) analytical methods, (ii.) empirical predictions, (iii.) boundary integral equation methods (BIEM), and (iv.) Navier-Stokes equation methods (NSEM) [12]. They observed that the high computational costs of NSEM may be reserved for nonlinear phenomenon such as wave-breaking, over-topping, and viscous damping effects are significant.

This work uses BIEM to simulate a surge-type terminator device. While Bernard Le Méhauté (see Chapter 11. and Chapter 15. in [13]) outlined the limitations of potential flow theory, WEC modeling using the linear potential flow theory has been extensively verified, and validated for terminator-type devices [5, 6, 11, 12, 14, 15].

Using the linear potential theory has certain practical advantages; the linear potential theory can be used to develop equations of motion in frequency and in time domain, such that, additional forces and loads can be easily incorporated in the model. Linear potential theory based models can be integrated with realistic multibody dynamical systems and enable a WEC model that is capable of modeling real-time control, and grid integration. A linear potential theory model can be deployed on off-shore WEC controllers; therefore, can adapt to changing wave-fields in real-time. Furthermore, a linear potential theory based model can be scaled from models to prototypes - with relatively modest changes in computational costs. These advantages, however, can be best leveraged by using a time-domain multibody solver. To that end, The National Renewable Energy Laboratory (NREL) and Sandia National Laboratories (SNL) developed WEC-Sim - an open-source software developed in MATLAB-Simulink, using its Simscape multibody packages [16].

Whittaker and Folley discussed the development of surge wave energy converters that extract energy using the incoming wave energy primarily in the surge mode [5]. Their work at Queen's University Belfast led to the development of the Oyster WECs which are analytically similar to the VGOSWEC (Variable Geometry Wave Energy Converter) discussed in this work. Kurniawan

and Moan characterized a pitching flap-type WEC and developed an analytical framework to evaluate energy extraction performance [17]. Their work showed that when the pitching flap is not perpendicular to the incoming wave, the structural loads are reduced. They discussed that the added-mass and radiation damping reduce for non-perpendicular flaps due to a pressure reduction along the prevailing wave heading. This observation is in concurrence to the structural load reduction strategies of VGOSWECs. Note, both [5] and [17] use linear potential flow theory. Linear potential theory can model the aggregate hydrodynamic effects such as the Froude-Krylov forces and the radiation forces but can only accommodate approximations for viscous effects, and other local effects such as vortex shedding. These additional phenomenon can impact motion through viscous losses, over-topping, and local pressure drops.

A more accurate analysis requires Computational Fluid Dynamics (CFD) based numerical modeling. Wei et al. developed CFD models for an OSWEC device, and discussed: (i) the viscous effects while the device oscillates in normal operating conditions [14], and (ii) the slamming effects and device survivability in extreme wave conditions [15]. In [14], they demonstrate that when compared to the hydrodynamic forces, the viscous forces are negligible at model scale and even more insignificant at full scale. However, their work does expose the inadequacy of linear potential flow theory when it comes to modeling over-topping and slamming. They simulated three cases with different damping forces at the hinge, (i) undamped, (ii) damped, and (iii) infinitely damped, i.e., fixed flap. This work considered similar cases to evaluate the effect of PTO damping on structural loads. This work used WEC-Sim to capitalize on the following features; (i.) a wide library of joints and constraints that can be used to customize the system dynamics - its degrees of freedom and relative motion of its different components, (ii.) incorporating a Power Take-Off (PTO) to the system dynamics, and be able to simulate a wide range of PTO characteristics, and (iii.) evaluate loads at different locations of the system and assess the trade-off between system performance and its structural loads. Additionally, an important advantage of developing a time-domain model using WEC-Sim is that the same model can be used for real-time control of the VGOSWEC in an experimental setting. While, the limitations of linear potential theory prevented reliable modeling of extreme conditions, over-topping, and viscous-damping - such shortcomings are out-weighed by the analytical versatility of linear potential theory based models and its validity for most of the operational conditions. The most compelling advantage of using WEC-Sim is the significantly lower computational costs, when compared to CFD or SPH based methods. This allows simulations of a wide variety of design variables, wave-conditions, and PTO mechanisms. The focus of this work is to present analyses of the initial design space rather than improving model accuracy - which can be the next stage that uses high fidelity models capable of simulating extreme conditions, over-topping, and viscous-damping.

Nevertheless, confidence in the analyses presented here can be justified by the in-depth investigation by Wei et al. - comparing CFD models with linear theory based models [14, 15]; and other works involving verification and validation of such models [18, 19]. This work investigates the effect of PTO damping on the VGOSWEC dynamics, and models similar cases using linear potential flow theory. Some of the key findings from the case case studies in [14], that are relevant to this work are,

1. The hydrodynamic pressure force, and the hinge damping force dominate the flap dynamics,
2. The undamped flap has a greater pressure difference between the fluid on the sea-facing and land-facing sides of the flap,
3. The damped and fixed flaps drag more water and have a greater fluid velocity around the flap,

4. The vorticity behavior and the direction of vortex flow is dependent on the relative motion of the flow and the flap. This relative motion results in opposite directions of the fluid flow for the fixed flap case (infinite damping), and the free-wheeling flap case (undamped),
5. The viscous effects are localized to the edges of the flap and are dominated by hydrodynamic forces even at a scale of 100 times that of the baseline cases modeled.

The relevance of the above listed observations to this work would be discussed in Section 6. Furthermore, Wei et al. in [15], discuss the CFD analysis of the OSWEC device in extreme wave conditions, and simulate the slamming effects. Wei et al. and Henry et al. observe that the slamming event occurs when the flap impacts the free-surface of water when there is pressure drop on the sea-facing side due to a wave trough [15, 20]. Wei et al. also note that the peak pressure exerted on the flap is approximately at the center of the flap. Note, the VGOSWEC discussed in this work allows wave transmission and thereby pressure relief - reducing the probability of slamming events. Given the evidence for a smaller contribution of viscous effects, Wei et al. recognize that works by Renzie et al. succesfully model Oyster WECs using the linear potential theory - as individual devices, and as arrays [18, 21–23].

Development efforts towards floating OSWECs, and VGOSWECs have been carried out at National Renewable Energy Laboratory (NREL) [24]. Yu et al. developed numerical time-domain models for a floating OSWEC, and estimated the Joint Probability Distribution (JPD) to characterize the device performance [11]. Tom et al. developed OSWECs with controllable flap that allow transmission of the incoming wave, as a pressure-relief to mitigate structural loads in extreme conditions, to enhance device performance, and reduce the probability of slamming and overtopping [25–28]. In the numerical models discussed in [25–28] the VGOSWEC is simulated at the scale of the Oyster WEC - approximately $10\ m$. Note, Henry optimized the OSWEC geometry and demonstrated that the OSWEC performance can be increased, and the viscous losses reduced if the flap cross-section was more curved, effectively using an elliptical cross-section [29]. This finding supports the choice of elliptical cross-sections of the controllable flaps in the VGOSWEC, so as to entail greater performance and lower viscous drags.

Detailed description of the VGOSWEC, and the operation of its controllable flaps can be found in [26]. Tom et al. developed active wave-by-wave control for varying the angular configuration of the flaps on the VGOSWEC to maximize power while considering the corresponding structural loads [28]. In [28], Tom et al. take a nuanced optimization approach to control the VGOSWEC configuration to strike a balance between the maximum power produced and the associated structural loads depending on the prevailing wave conditions. This was done by formulating the optimizer's cost function such that appropriate numerical weights would allow shifting priorities between the device performance or its survivability.

REMOVED The design workflow for a WEC is constrained by factors such as structural load and control. Therefore, WEC design requires robust support structures that can withstand extreme weather events. Adaptability to the wave loads on the structure is a critical design constraint that should be part of the WEC design process. Tom et al. discussed a variable-geometry oscillating surge wave energy converter (VGOSWEC), which was developed at the National Renewable Energy Laboratory (NREL) [25]. A VGOSWEC is an oscillating surge WEC (OSWEC) with controllable flaps to alter the device geometry, and thus the device hydrodynamics, to reduce loads on the WEC support structure [24, 28, 30]. The variable-geometry feature of the VGOSWEC expands the range of operable sea states.

Kelly et al. simulated the performance of VGOSWEC devices at three different sites across

the United States and assessed the load-shedding advantages of variable-geometry WEC designs [30]. Choiniere et al. developed a VGOSWEC that can reduce the loads on the supporting structure using controllable load-relief flaps on the VGOSWEC when a threshold loading is experienced [19]. Sea-keeping of WECs is challenging and mitigating structural loads during extreme conditions and long-term structural fatigue ameliorates logistic costs. While a techno-economic analysis is necessary to objectively quantify the advantages of the load-shedding mechanisms of the VGOSWEC; the ability to control structural loads can potentially extend the overall lifetime of the VGOSWEC.Therefore, the variable geometry can help design better-informed control strategies in tandem with the PTO-based control.

The range of deployment sites can be further expanded by mounting VGOSWEC devices on a raised platform. Such design configurations have been researched for an OSWEC-type device. Burge et al. showed that mounting an OSWEC on a raised platform expands the number of available installation sites, with potentially higher energy yields [31]. They analyzed an OSWEC mounted on a raised platform and explored the effect of lowering pressure plates and changing the parameters of the supporting foundation to maximize performance at different operating conditions and wave climates [31].

The work presented here models a raised-platform-mounted VGOSWEC that emulates the model-scale tests completed at the University of Massachusetts Amherst. These tests were funded by the U.S. Department of Energy Office of Technology Transitions Technology Commercialization Fund Award [31–33]. The hypothesis for this work is to demonstrate that controllable flaps on a VGOSWEC reduce the loads experienced by the supporting raised platform. A WEC-Sim numerical model [16] is used to analyze the natural periods, response amplitude operators (RAOs), and loads on the support structure to determine if the hypothesis holds true.

The objectives of this work are to investigate:

1. The validity of the hypothesis that allowing water transmission through the VGOSWEC leads to structural load-shedding at wave-tank testable model scale,
2. The factors contributing to structural loads; specifically, the VGOSWEC configuration, the PTO damping, and the different natural periods of each VGOSWEC configuration,
3. The performance sacrifices when the VGOSWEC is in load-shedding configurations.

The rest of the paper is organized as follows: Section 2 describes the VGOSWEC device, its geometry, its equations of motion, and its hydrodynamic characteristics; Section 3 describes the time-domain modeling of the VGOSWEC device, along with its free-decay characteristics; Section 4 then shows the influence of varying the water transmitted through the VGOSWEC, and Section 5 investigates the effect of varying the PTO damping; this is followed by the discussion and conclusions in Section 6 and Section 7.

2 DESCRIPTION OF A RAISED VGOSWEC

The raised VGOSWEC considered in this study is a two-body system, as illustrated in Figure 1. The device comprises a paddle of width 0.4 m and height 0.5 m that is mounted on a monopile such that the paddle is free to pitch about an axle running through the paddle near its bottom surface. The monopile is rigidly attached to the bottom surface of the wave tank. The paddle has a series of four flaps that can be configured to be: (i) completely closed, (ii) partially open at some predefined angle, and (iii) completely open. The objective of the configurable flaps is to reduce the surface pressure exerted on the VGOSWEC to reduce the incoming excitation forces on the paddle so

that the loads acting on the monopile are reduced. A rotary PTO is implemented using a spring with no damping. Table 1 shows the physical parameters of the paddle used in the numerical models that follow. The pertinent equations of motion are discussed in Section 2.1, followed by the development of a numerical time-domain simulation using WEC-Sim in Section 2.2.

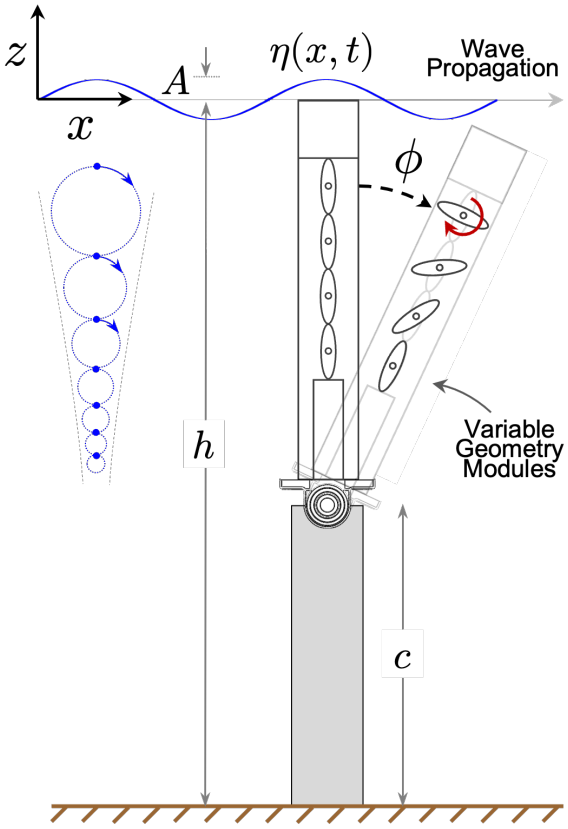

Fig. 1. Schematic representation of the VGOSWEC, where h is the water depth, c is the height of the support structure, η represents the wave elevation A is wave amplitude, and ϕ represents the pitch angle. The flaps are controllable such that the 0° configuration represents the completely closed configuration, and the 90° configuration represents the completely open configuration.

2.1 VGOSWEC Equation of Motion, Surge Foundation Force, and Pitch Foundation Moment

The dynamics of the two-body system simulated here are mutually coupled. The equations of motion for N coupled bodies will comprise $6N \times 6N$ modes for the phenomena affected by the floating body and $6N \times 1$ modes for the incident excitation force because it is the input to the system independent of the body response and its couplings. Therefore, the radiation damping, added mass, and hydrostatic force matrices in this case will be 12×12 while the excitation force coefficient matrix will be 12×1. In the discussion that follows, the modes are ordered as surge, sway, heave, roll, pitch, and yaw. Modes 1–6 represent the paddle's modes, and modes 7–12 correspond to the monopile. Therefore, the surge mode for the paddle will be represented as

Property	Variable	Value	Unit
Width	w	0.4	m
Height	H_p	0.5	m
Thickness	t	0.076	m
Paddle geometry	-	-	-
	Cross section	ellipse	-
	Number	4	-
	Paddle length	0.349	m
	Paddle cord	0.076	m
	Paddle thickness	19	mm
Body mass	m	6.30	kg
Displaced volume	$\forall$	7395	cm^3
Center of gravity*	r_g	0.274	m
Center of buoyancy*	r_b	0.293	m
Moment of inertia	I_{55}	0.962	kg m^2
Foundation geometry	-	cylindrical	-
Foundation radius	r_f	0.05	m
External springs	C_{ext}	6.57	kg m^2 s^{-2}

Table 1. Geometric and Inertial Properties of the VGOSWEC. * denotes measurements from the hinge.

the ordered pair, $1,1$, the surge mode of the monopile will be represented as $7,7$, and the coupled modes will be represented as an ordered pair made up from a combination of modes 1–6 and 7–12. The notations for the rest of the paper will have two-digit ordered pair subscripts representing the corresponding mode. The auto-coupled terms (i.e., the body-only modes such as surge, heave, and pitch) make up the diagonal terms in the $6N \times 6N$ matrices while the coupled modes make up the corresponding off-diagonal terms.

As shown in [30], the VGOSWEC linear pitch equation of motion about the hinge can be modeled in the frequency domain as

$$\frac{\xi_{5,5}}{A} = \frac{E_{5,5}}{[C_{5,5} - \omega^2 (I_{5,5} + \mu_{5,5})] + i\omega [\lambda_{5,5} + \lambda_g]} \tag{1}$$

where A is the amplitude and ω the angular frequency of the incident wave, $\xi_{5,5}$ is the complex pitch displacement amplitude, $E_{5,5}$ is the complex pitch excitation torque per unit wave amplitude, C_{55} is the pitch restoring coefficient, I_{55} is the pitch mass moment of inertia, μ_{55} is the pitch radiation added moment of inertia, λ_{55} is the pitch radiation damping, and λ_g is the linear, rotational PTO damping. The hinge that the VGOSWEC rotates about will have to withstand surge forces due to the surge excitation force on the VGOSWEC and from the radiation surge-pitch coupling forces [30]

such that

$$E_{r1,1} + E_{1,1} = \left[-\omega^2 \mu_{1,5} + i\omega\lambda_{15}\right] \frac{\xi_{5,5}}{A} \tag{2}$$

where $E_{r1,1}$ is the hinge reaction force per unit wave amplitude in the surge mode, $\mu_{1,5}$ is the surge-pitch radiation added mass, λ_{15} is the surge-pitch radiation damping, and $E_{1,1}$ is the surge-wave excitation force, per unit wave amplitude. The monopile foundation is assumed to be sufficiently rigid to prevent any oscillatory motion, thereby eliminating any radiation forces from the foundation. From this approximation, a summation of the surge forces at the base of the monopile foundation can be modeled as

$$-E_{r1,1} + E_{7,7} + E_{r7,7} = 0 \rightarrow E_{r7,7} = E_{r1,1} - E_{7,7} \tag{3}$$

where $E_{r7,7}$ is the foundation reaction force in the surge mode. Substituting Equation (2) in Equation (3) and rearranging,

$$E_{r7,7} = -E_{1,1} - E_{7,7} + \left[-\omega^2 \mu_{1,5} + i\omega\lambda_{1,5}\right] \frac{\xi_{5,5}}{A} \tag{4}$$

where $E_{7,7}$ is the surge excitation force on the monopile foundation. Equation (4) shows that the foundation reaction force in surge mode has contributions from the surge excitation force on the VGOSWEC, the surge-pitch radiation force on the VGOSWEC, and the surge excitation force on the monopile.

The moment at the base of the monopile foundation will also include contributions from the excitation loads on the centers of gravity of the paddle and the monopile, along with the VGOSWEC radiation forces, such that

$$-E_{r1,1}c + E_{7,7}\frac{c}{2} + E_{9,9} + E_{r9,9} = 0 \tag{5}$$

$$\rightarrow E_{r9,9} = E_{r1,1}c - E_{7,7}\frac{c}{2} - E_{9,9} \tag{6}$$

where $E_{9,9}$ is the pitch-wave excitation moment on the monopile foundation and $E_{r9,9}$ is the foundation reaction moment in the pitch mode. Equation 6 can be expanded using Equation (4) such that the contributions to the monopile pitch reaction moment, $E_{r9,9}$, can be expressed as

$$E_{r9,9} = \left(-E_{1,1} + \left[-\omega^2 \mu_{15} + i\omega\lambda_{15}\right] \tfrac{\xi_{5,5}}{A}\right) c - E_{7,7}\tfrac{c}{2} - E_{9,9} \tag{7}$$

$$E_{r9,9} = -E_{1,1}c + \left[-\omega^2 \mu_{15} + i\omega\lambda_{15}\right] \tfrac{\xi_{5,5}}{A} c - E_{7,7}\tfrac{c}{2} - E_{9,9} \tag{8}$$

$$E_{r9,9} = -E_{9,9} - \tfrac{c}{2}\left(2E_{1,1} + E_{7,7}\right) + \left[-\omega^2 \mu_{15} + i\omega\lambda_{15}\right] \tfrac{\xi_{5,5}}{A} c \tag{9}$$

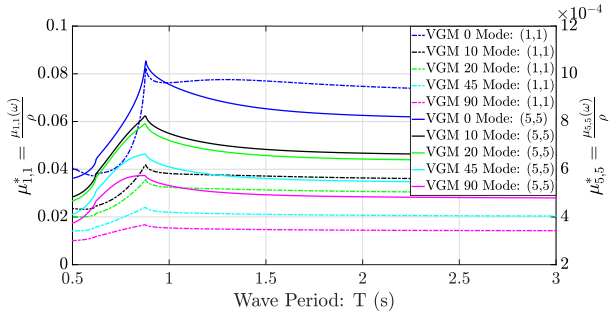

(a) The comparison of surge (left vertical axis) and pitch (right vertical axis) added mass coefficients for the paddle.

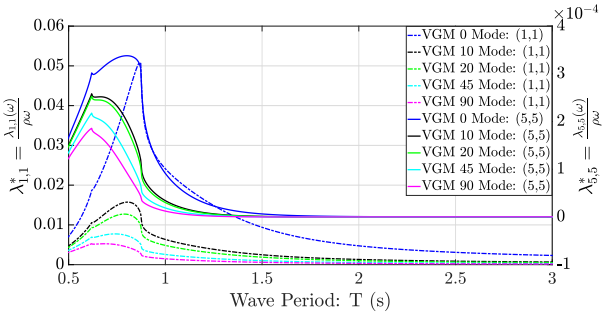

(b) The comparison of surge (left vertical axis) and pitch (right vertical axis) normalized radiation damping coefficients for the paddle.

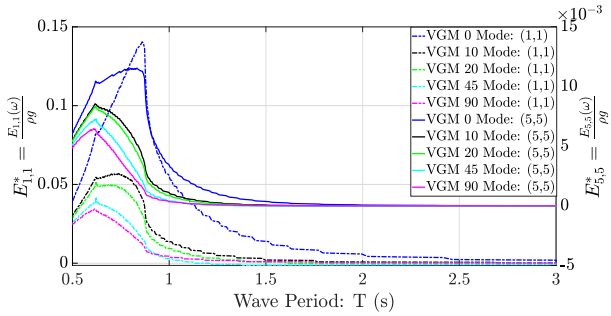

(c) The comparison of surge (left vertical axis) and pitch (right vertical axis) normalized excitation force coefficients for the paddle.

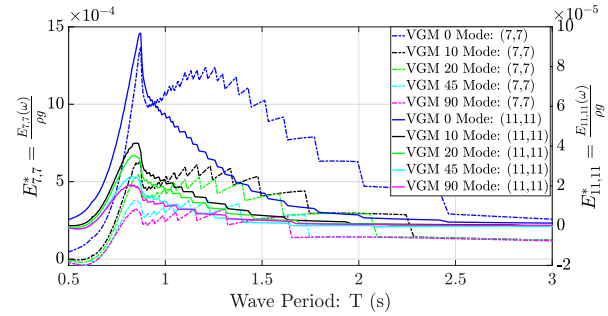

(d) The comparison of surge (left vertical axis) and pitch (right vertical axis) normalized excitation force coefficients for the monopile.

Fig. 2. The comparison of normalized hydrodynamic coefficients.

2.2 VGOSWEC Hydrodynamics Coefficients

A floating body in water experiences the excitation force (Froude-Krylov force), the diffraction force, the hydrostatic force, and the radiation force. The diffraction and the radiation problem is solved by calculating the frequency-dependent hydrodynamic coefficients to write the frequency-domain equations of motion. The time-domain models discussed in Section 3 are then developed using the impulse response functions calculated using the Fourier transforms of the frequency-dependent terms.

The hydrodynamic coefficients for this paper were calculated using the boundary-element-method-based commercial software WAMIT. The hydrodynamic and hydrostatic forces are calculated by discretizing the body geometry in bounded panels. The surface integrals of the pressure due to the incoming wave manifests as the excitation force (or the dynamic Froude-Krylov force), and the subsequent scattered wave diffracted by the body manifests as the diffraction force. The hydrostatic force represents the buoyancy force calculated as the surface integral of the pressure exerted on the body due to water's reaction force to the body's weight force, and the radiation force is the surface integral of the pressure exerted on the body as a reaction to the radiated wave field generated by the body when it is in motion.

The hydrodynamic coefficients for five VGOSWEC configurations ($0^\circ, 10^\circ, 20^\circ, 45^\circ,$ and 90°) are shown in Figure 2(a)–2(d). The VGOSWEC hydrodynamic coefficients decrease as the paddle is opened from the 0° configuration to the 90° configuration. Also, the normalized hydrodynamic coefficients in pitch mode were found to be an order of magnitude smaller than those in surge mode. Figure 2(a)–2(d) compares the VGOSWEC surge and pitch hydrodynamic coefficients for

(i) the paddle at all geometric configurations and (ii) the monopile.

Notice that the peaks of the lobes align obliquely for all the cases in Figure 2(a)–2(d) around 7 rad/s (0.897 s wave period). This indicates the effect that the wave-tank walls or the wave-tank geometry and depth may have on the hydrodynamic coefficients. The WAMIT model included the sidewalls and the bottom surface of the wave tank to emulate the wave-tank experimental setup as closely as possible with this approach. Although the boundary element method calculations in WAMIT modeled the wave tank's sidewalls, it did not model the walls parallel to the hinge axis. This could potentially introduce some divergence from experimental results.

It can be observed that there is a significant decrease in the hydrodynamic coefficients from the 0° configuration to all of the other configurations. Recall that the hydrodynamic coefficients are calculated as the surface integrals of the corresponding wave potential field. This drop can be attributed to the drop in the pressure exerted on the paddle as the flaps are opened. The hydrodynamic coupling between the paddle and the monopile introduced this effect onto the hydrodynamic coefficients of the monopile as well. Since the hydrodynamic forces are calculated using the hydrodynamic coefficients, it can be hypothesized that the time-domain modeling will show similar patterns in the loads exerted on the foundation (i.e., reducing in magnitude as the flaps are opened to the fully open 90° configuration).

The loads experienced at the foundation will have their moment arm from the foundation to the centers of gravity of the paddle and monopile, so the moments at the foundation will have contributions from the surge and pitch loads. The hydrodynamic coefficients are calculated at the body's center of gravity, whereas the equations in Section 2.1 are calculated at the hinge, about which the paddle oscillates in pitch mode. The equations in Section 2.1, therefore, need the appropriate transpositions to the hinge.

3 WEC-SIM VGOSWEC MODEL DEVELOPMENT

WEC researchers typically use the Cummins equation to model the WEC dynamics in the time domain [8,10,34]. The WEC model was simulated using WEC-Sim, which is a time-domain solver for WECs developed jointly by NREL and Sandia National Laboratories [16]. The hydrodynamic coefficients were postprocessed using the 'BEMIO' utility that is part of the WEC-Sim suite. The hydrodynamic coefficients, their corresponding impulse response functions, and relevant physical parameters were saved as data structures in an '*.h5' file and a MATLAB data file in the '*.mat' format. The WEC-Sim model then implemented the Cummins equation using a customized library of Simulink blocks in the Simscape multibody library. The PTO was modeled using a rotational PTO block from the WEC-Sim library. The PTO stiffness and damping values were defined such that they were consistent with the planned experiments [31]; the PTO stiffness was set at $K_{PTO} = 6.57$ N/m, and the PTO damping was set at $C_{PTO} = 0$ N·s/m. The damping was set at 0 to investigate the effect of changing the geometric configuration alone. The effect of changing PTO damping is discussed in Section 5.

3.1 Free-Decay WEC-Sim Simulations

Free-decay simulations were conducted to determine the natural frequency, ω_n, and damping ratio, ζ, of the VGOSWEC in different geometric configurations. The natural frequencies for each geometry were obtained by performing a fast Fourier transform (FFT) on the time history of the free-decay pitch responses. Table 3.1 shows that the natural frequency increases as the flaps on the VGOSWEC are opened, indicating that the net added mass moment about the hinge has

Geometric Configuration	ω_n [rad/s]	T_s [s]	$\zeta \times 10^{-4}[-]$
VGM 0	1.07	5.86	5.8
VGM 10	1.46	4.29	4.3
VGM 20	1.57	4.01	4.1
VGM 45	1.84	3.42	3.5
VGM 90	2.10	2.99	3.2

Table 2. Natural frequency for each VGOSWEC geometric configuration measured from free-decay simulations.

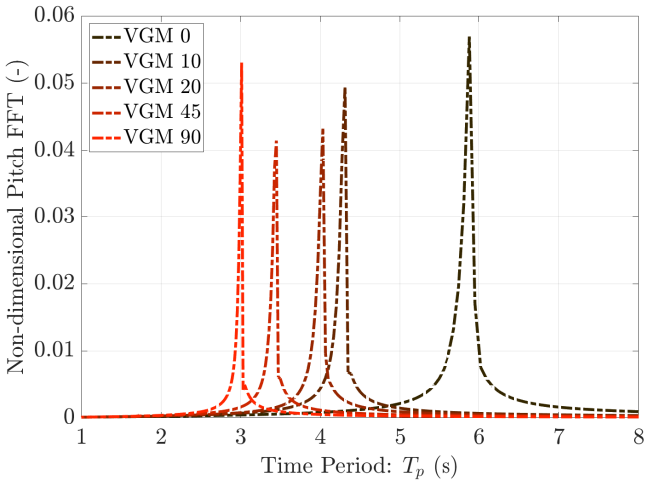

Fig. 3. The nondimensionalized FFT for the pitch displacements, where the nondimensional pitch displacements were $\xi_5{}^* = \frac{\xi_5}{ka}$. The frequency corresponding to the peaks represents the natural frequencies.

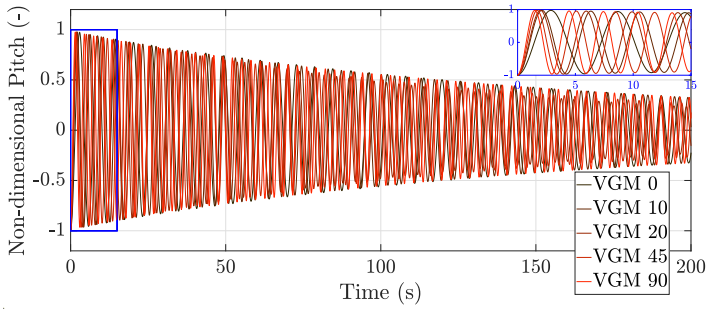

Fig. 4. The nondimensionalized time series for the pitch displacements.

been reduced. The decrease in added mass emboldens the hypothesis that the opening of the flaps of the VGOSWEC decreases the structural loading on the foundation. The natural frequency of the VGOSWEC in different geometric configurations was determined by using the frequencies

corresponding to resonant peaks in the FFT. Figure 3 shows the FFTs for a free-decay test when the initial displacement is 10.4°.

Table 3.1 also shows the damping ratio, ζ, calculated using the log-decrement method. The damping ratio decreases by $\approx 50\%$ from the 0° configuration to the 90° configuration. This corroborates the decline in radiation damping coefficients in Figure 2(c).

4 EFFECTS OF VARYING THE GEOMETRY

This section would discuss the effect of varying the geometry for different values of PTO damping. This section would first show the bounding cases of zero PTO damping and infinite PTO damping, followed by a sweep of PTO damping values.

4.1 At Zero PTO Damping

The VGOSWEC geometry was varied such that the flaps were completely closed in the 0° configuration to completely open in the 90° configuration, with results shown in Figures 5–7. Figures 5–7 show that although the pitch displacements increase as the flaps of the VGOSWEC are opened, the structural loads experienced at the bottom of the foundation decrease between the time periods 0–2 s. Note that the VGM 90 configuration has its natural frequency at a wave period of 2.99 s. These loads are exacerbated because there is greater motion, and the phase difference between motion and excitation increases. Tom et al. (2017) show that the resonance condition shifts the amplitude response relative to the wave phase, which causes an amplification of loads on the foundation [28].

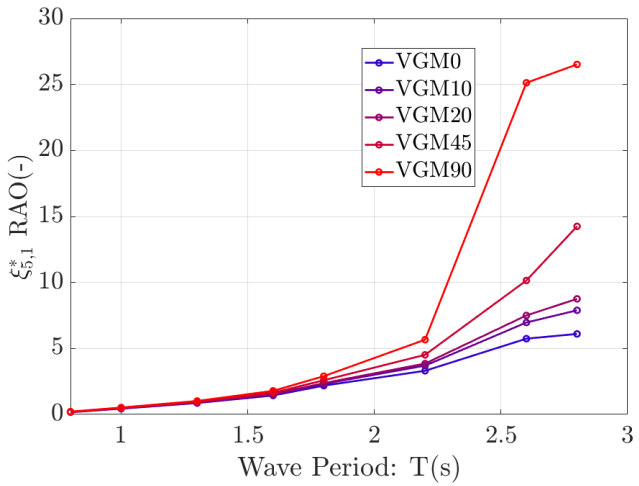

Fig. 5. Comparison of nondimensional pitch displacements across different geometric configurations of the VGOSWEC. The pitch displacements were nondimensionalized using the wave number k and wave amplitude a such that the non-dimensional Pitch $RAO^* = \frac{\xi_5}{ka}$. The PTO damping for this case was set to zero.

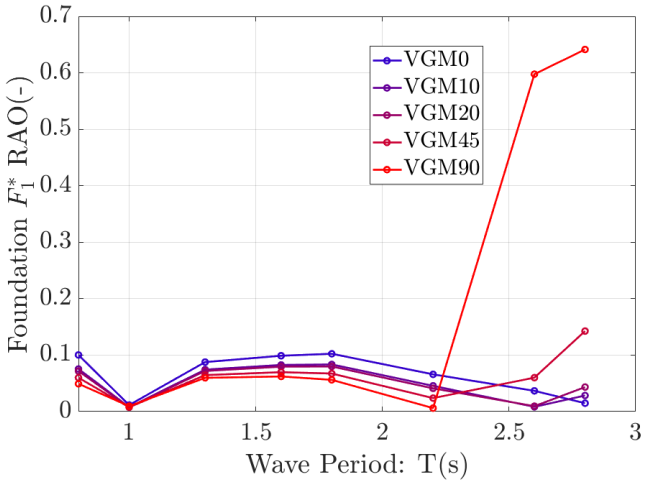

Fig. 6. Comparison of nondimensional surge force across different geometric configurations of the VGOSWEC, where $F_1^* = \frac{F_1}{2}\rho g w H_p a$. The PTO damping for this case was set to zero.

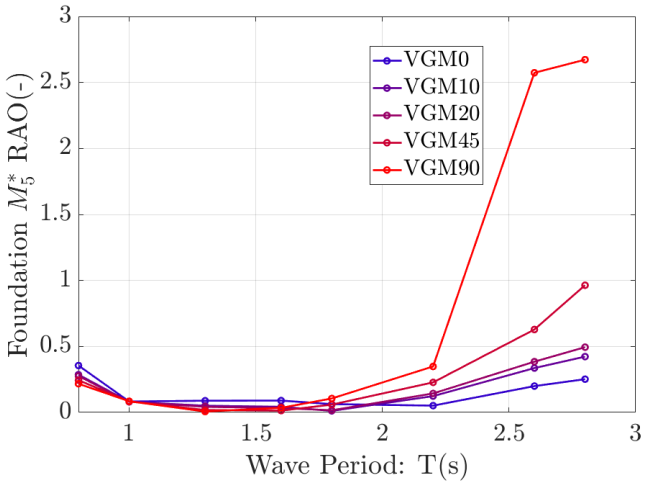

Fig. 7. Comparison of nondimensional pitch moment on the foundation across different geometric configurations of the VGOSWEC, where $M_5^* = \frac{F_5}{\frac{1}{6}\rho g w H_p^2 a}$. The PTO damping for this case was set to zero.

4.2 At Infinite PTO Damping

As the PTO damping coefficient, λ_g, approaches infinity, the VGOSWEC will essentially be locked in place atop the foundation, and the only forces and moments on the foundation will be from the wave excitation forces and moments. This follows from Equation 1, where as the PTO damping coefficient approaches infinity the pitch RAO approaches 0 ($\lambda_g \to \infty \implies \xi \to 0$). Recall that Equation 4 gives the relation for the reaction loads on the foundation; the right side of the equation has contributions from the excitation loads. The configurations with higher excitation load hydrodynamic coefficients will lead to the highest loads on the foundation. Therefore, since the 0° configuration has the largest wave excitation coefficients, it experiences the largest loads

at the base of the foundation when the connection between the VGOSWEC and the foundation is rigid, and the paddle is locked in place as shown in Figures 8–10. However, locking the 90° configuration leads to the lowest surge force and pitch moment on the foundation compared to when the other configurations are held fixed.

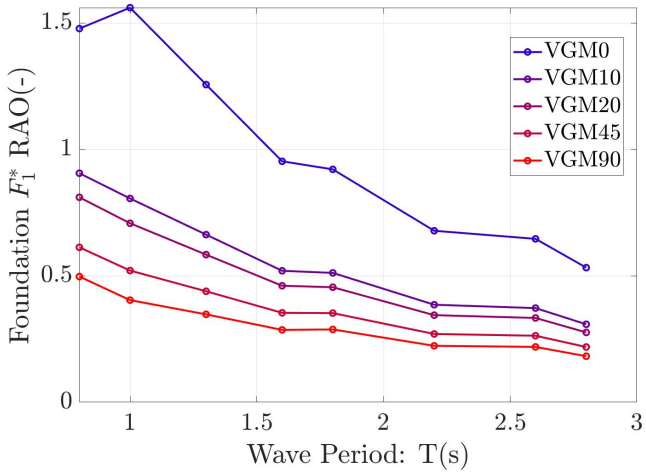

Fig. 8. Surge force on the foundation at infinite PTO damping.

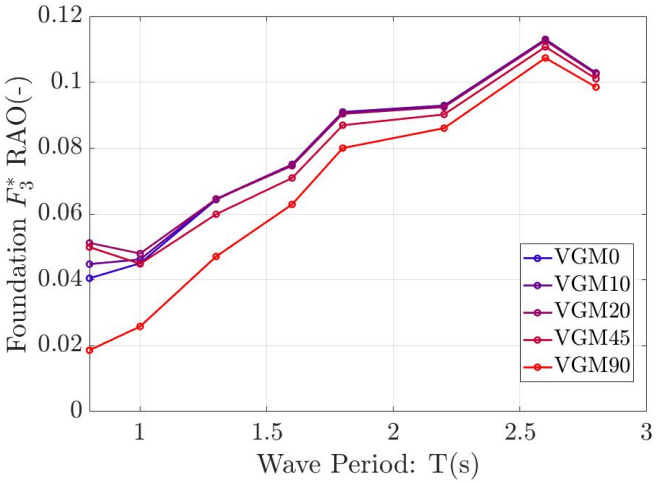

Fig. 9. Heave force on the foundation at infinite PTO damping.

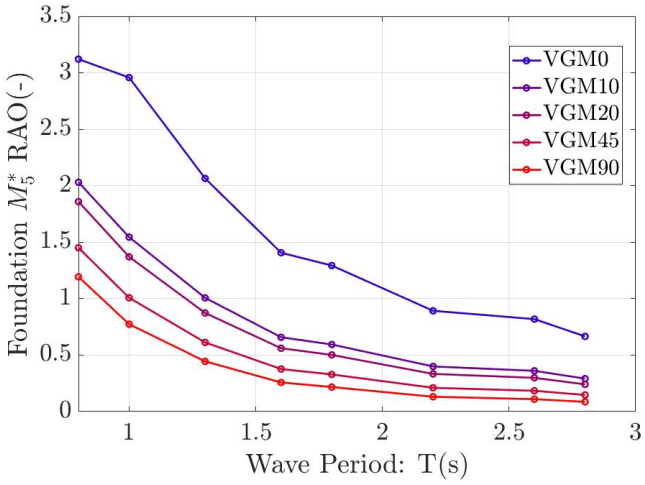

Fig. 10. Pitch moment on the foundation at infinite PTO damping.

5 EFFECTS OF VARYING THE PTO DAMPING

Additional simulations were performed by varying the PTO damping coefficients from 0.5 N·s/m to 5.0 N·s/m to observe their effect on pitch displacement and foundation loads corresponding to the different geometric configurations. Figures 11–15 show the effect of varying PTO damping on the nondimensionalized pitch displacement of the paddle, the nondimensionalized surge force, and the pitch moment on the foundation.

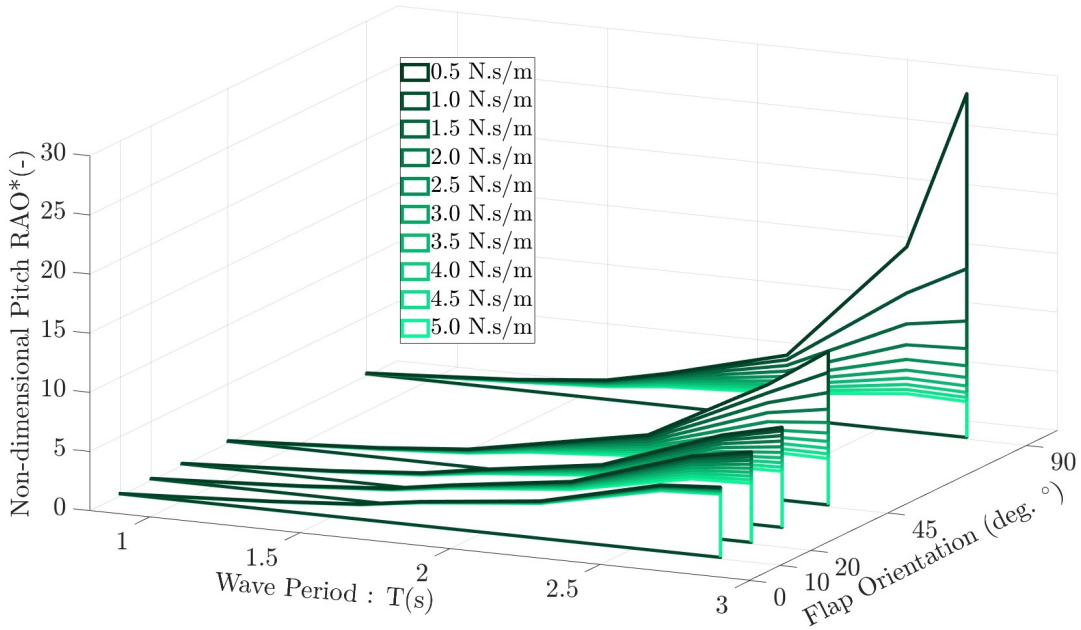

Fig. 11. Comparison of normalized pitch displacement when the PTO damping is swept from 0.5 N·s/m to 5.0 N·s/m.

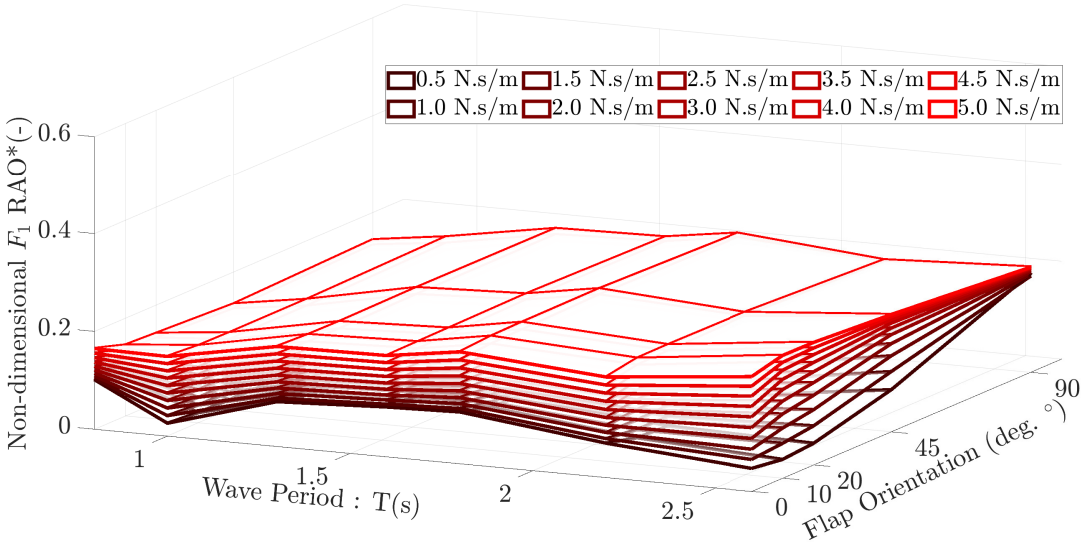

Fig. 12. Comparison of normalized surge force on the foundation when the PTO damping is swept from 0.5 N·s/m to 5.0 N·s/m.

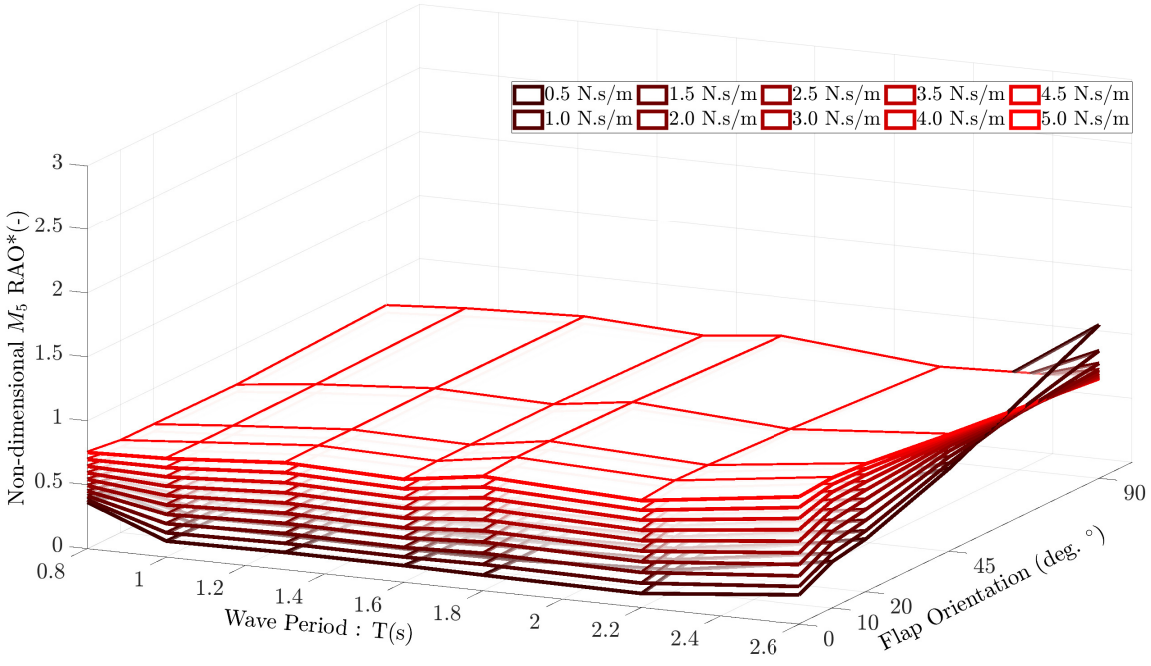

Fig. 13. Comparison of normalized pitch moment on the foundation when the PTO damping is swept from 0.5 N·s/m to 5.0 N·s/m.

The effect on the nondimensionalized average power is shown in Figure 16(a) and 16(b). When the PTO damping coefficient was increased, the surge force and pitch moment measured at the base of the foundation also increased, with the largest loading occurring for the $0°$ configuration. The power plots in Figure 16(a) and 16(b) show that the PTO generated the highest power from

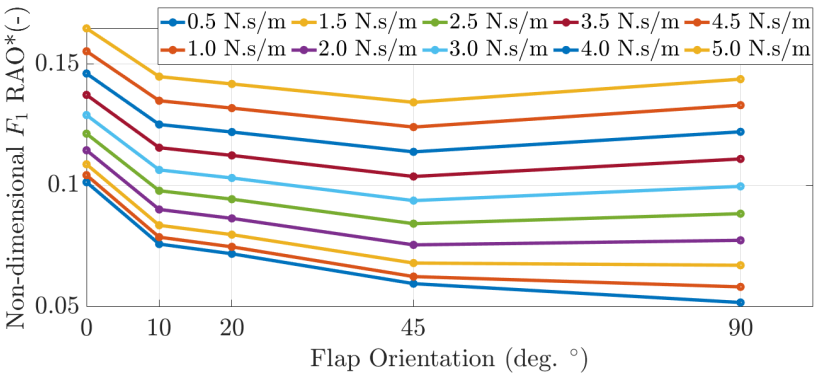

Fig. 14. Comparison of normalized surge force on the foundation when the PTO damping is swept from 0.5 N·s/m to 5.0 N·s/m at a wave period of 0.8 s.

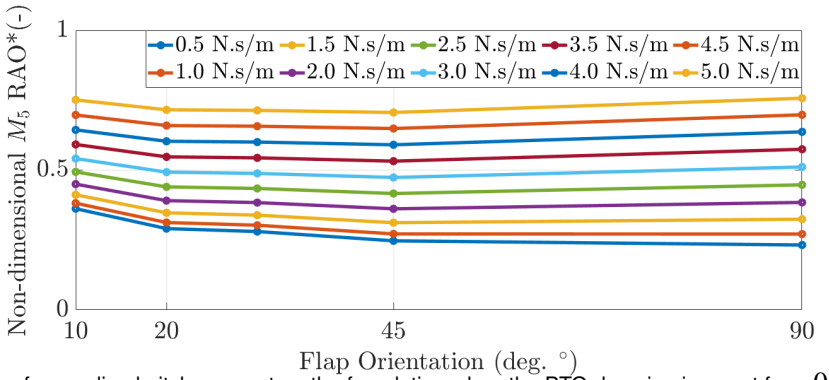

Fig. 15. Comparison of normalized pitch moment on the foundation when the PTO damping is swept from 0.5 N·s/m to 5.0 N·s/m at a wave period of 0.8 s.

the 0° configuration with the largest damping coefficients. Therefore, the higher PTO damping coefficients and the 0° configuration can be used as an optimum, and it is likely that the largest damping value for power production while opening the flaps can achieve the desired load shedding by reducing the forces and moments on the foundation.

In Figure 16(a) and 16(b), the average power is normalized by dividing the average power produced by the paddle (using the PTO force and the oscillation velocity) by the average incident power. The average incident power can be expressed as

$$\bar{P}_I = \bar{e} v_g, \text{ where } \bar{e} = \frac{1}{2}\rho g A^2(\omega) \text{ and, } v_g = \frac{1}{2}\frac{\omega}{k} \quad 1 + \frac{2kh}{\sinh 2kh}\Bigg)\Bigg(\tag{10}$$

where $\bar{e}$ is the energy density, and v_g is the group velocity [1, 8, 9, 13, 35]. The nondimensionalized average power is then calculated using

$$\bar{P}^* = \frac{\bar{P}}{\bar{P}_I} \tag{11}$$

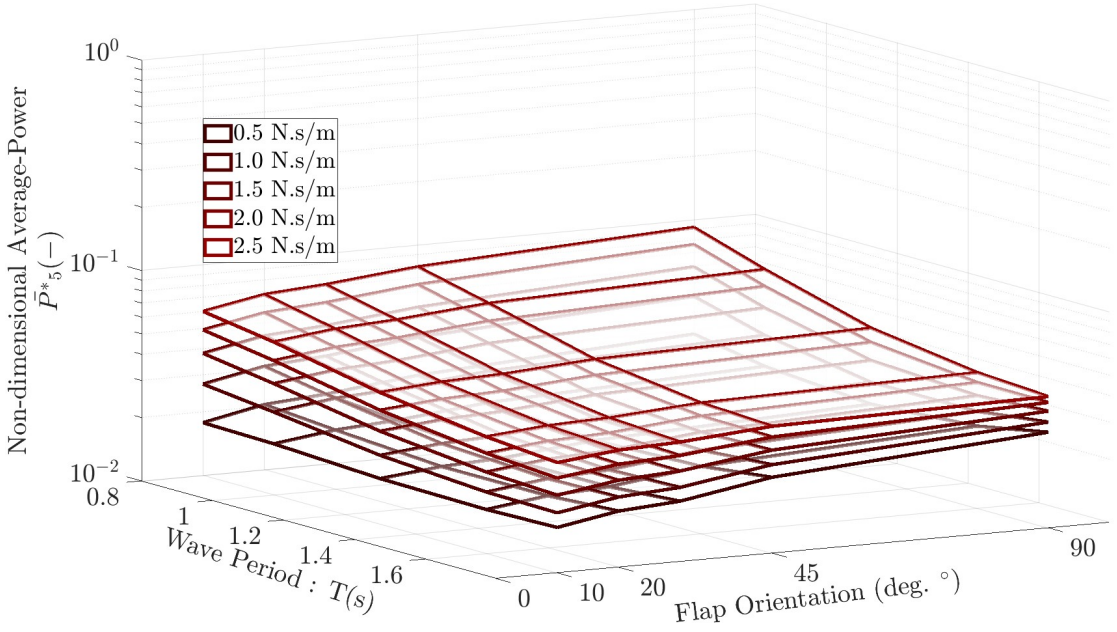

(a) $\bar{P}^*_5$ when the PTO damping is swept from 0.5 N·s/m to 2.5 N·s/m.

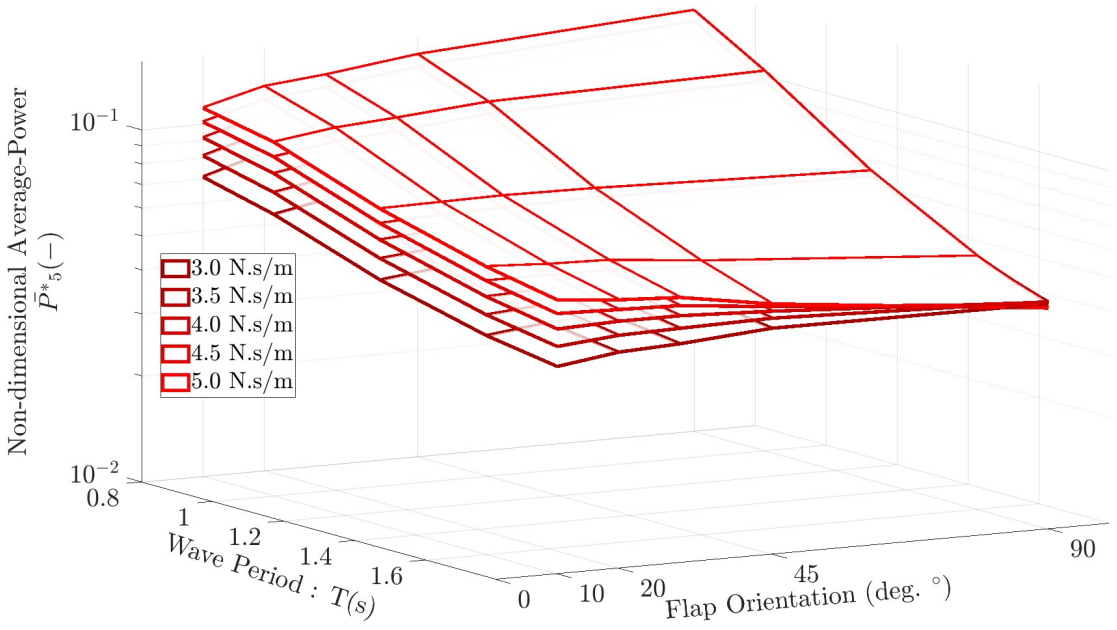

(b) $\bar{P}^*_5$ when the PTO damping is swept from 3.0 N·s/m to 5.0 N·s/m.

Fig. 16. Comparison of normalized average power, $\bar{P}^*_5$.

The 90° configuration case oscillates significantly less than the 0° configuration case for the same PTO damping value while experiencing the same wave conditions.

The WEC-Sim results demonstrate that combined control of the flap orientation and the PTO damping coefficient can help limit loading on the supporting foundation design, which is expected to reduce the required materials and drive the cost of energy down.

6 DISCUSSION

A WEC needs to acclimatize to the harsh marine environment and weather events such as hurricanes and tsunamis. The structural loading imposed by the wave climate poses an existential challenge if the WEC structure fails to survive such conditions. Additionally, the fatigue due to structural loading over time also constrains the service life of the WEC. The VGOSWEC design modeled here can control the transmission of the incoming waves through the WEC structure, thereby extending the service life and reducing maintenance costs. The hydrodynamic coefficients calculated using WAMIT showed that the hydrodynamic coefficients decreased in magnitude as the flaps were opened. This decline can be attributed to the increased transmission of the incoming waves, thereby reducing the pressure experienced by the WEC structure.

Figures 12 and 13 show the effect of changing the PTO damping on the surge forces and pitch moment experienced at the base of the foundation. The structural loading trends support the hypothesis that opening the flaps of the VGOSWEC reduces the structural loads at the base of the foundation. The load-shedding hypothesis was also corroborated when the PTO damping was increased to infinity, such that the VGOSWEC was held fixed. Observe the reduction in the hydrodynamic loading at the base (Figures 8–10) of the supporting foundation as the VGOSWEC flaps are opened from the completely closed (90°) configuration to the completely open (0°) configuration. These trends satisfied the load-shedding motivation for varying the geometry of the VGOSWEC. Figures 14 and 15 show the foundation loads as the PTO damping is varied from 0.5 N.s/m to 5.0 N.s/m at a wave period of 0.8 s. At shorter waves and at lower PTO damping values, the load shedding for the 90° configuration is highest.

However, as the PTO damping is increased, the foundation loads for the 90° configuration increase with respect to the 45° configuration (while still lower than for the more closed configurations). This apparently anomalous behavior could be attributed to the resonance-induced increase in oscillations and foundation loads. The free-decay tests, completed using WEC-Sim, were used to determine the natural frequency of the VGOSWEC (when allowed to freewheel by setting the PTO damping to zero) in different geometric configurations. The natural frequency of each geometric configuration explains the increase in oscillations and loads in longer wave periods. Note that from the free-decay cases, the resonance period of the 90° configuration was lower than that of the other configurations (see Table 3.1). This causes an increase in loads for the 90° configuration at wave periods closer to its natural period.

The comparison of foundation loads for a shorter wave period (0.8 s in Figures 14 and 15) illustrates that the load shedding is highest for the 90° configuration for lower PTO damping coefficients; this trend is reversed for longer waves that are closer to the 90° configuration's natural period, as shown in Figures 12 and 13. However, overall, the foundation loads are lower for the completely open 90° configuration when compared to the completely closed 0° configuration.

The comparison of average power generated by the PTO is shown in Figure 16(b). Notice as the PTO damping coefficient, C_{PTO}, is increased, the average power also increases. This indicates that higher generated power corresponds to the increase in foundation loads. This trade-off

between power produced and foundation loads can be an important consideration for control. Further investigation of the PTO parameters could help balance the power generation objectives and the need for load shedding in extreme conditions,as discussed in [28]. Interestingly, the structural loads could be higher for open configurations if,

1. The PTO damping is below a threshold causing an increase in pitch velocity, making the product of damping and velocity higher than the less open configurations, i.e., the more closed configuration are damped more due to higher radiation damping,
2. The configuration is closer to its natural period.

Nevertheless, some advantages of the VGOSWEC are that they can reduce non-linear losses due to slamming, and viscous effects due to the pressure-relief homogenising the pressure differential between the sea-facing side and the coast-facing side. The vortices formed at each flap in the open configurations of the VGOSWEC may result in additional pressure-drop in the opposite direction of the relative motion between the flow and VGOSWEC. These pressure drop may further reduce the structural loads, as the fluid would exert lesser force on the device. This can be inferred from the work by Wei et al. in [14] and [15], when they point out that vortex flow causes an increase in fluid velocity, and so the resulting pressure drop may further help reduce structural loads.

7 CONCLUSIONS

The design parameters simulated here were based on the wave tank tests conducted at University of Masssachusetts, Amherst under the aegis of the Technology Commercialization Fund [32]. The simulation results here can therefore be validated using experimental data in the future. The hypotheses regarding load-shedding characteristics of VGOSWEC were originally developed for much larger full-scale devices. This work shows that the hypotheses will hold for devices that are smaller by an order of magnitude. The time-domain models developed in this work using WEC-Sim provided valuable insights into the dynamics of the VGOSWEC. The versatility to quantify loading at various locations on the WEC geometry can inform the design process before the logistically intensive experimental testing is conducted. This works shows that the loads experienced at the foundation of the support structure are related to the VGOSWEC oscillations in addition to the prevailing wave climate. The time-domain simulations corroborated the hypothesis that having controllable flaps that allow transmission of water can significantly reduce the loads on the supporting structure. Additionally, the loads experienced at the foundation of a VGOSWEC are also affected by dynamic response characteristics at natural periods and PTO design parameters. Future work could investigate VGOSWEC designs that incorporate PTO design and control for load shedding. Future VGOSWECs could also incorporate adaptability to changes in wave directions. Nevertheless, the capability to adapt device geometry expands the sites and conditions in which the VGOSWEC can operate.

ACKNOWLEDGEMENTS

This work was authored in part by the National Renewable Energy Laboratory, operated by Alliance for Sustainable Energy, LLC, for the U.S. Department of Energy (DOE) under Contract No. DE-AC36-08GO28308. Funding provided by the U.S. Department of Energy Office of Energy Efficiency and Renewable Energy Water Power Technologies Office. The views expressed in the

REFERENCES

[1] Korde, U. A., and Ringwood, J., 2016. *Hydrodynamic Control of Wave Energy Devices*. Cambridge University Press, Sept.

[2] Todalshaug, J. H., Ásgeirsson, G. S., Hjálmarsson, E., Maillet, J., Möller, P., Pires, P., Guérinel, M., and Lopes, M., 2016. "Tank testing of an inherently phase-controlled wave energy converter". *International Journal of Marine Energy,* ***15***, Sept., pp. 68–84.

[3] Salter, S., Jeffery, D., and Taylor, J., 1976. "The architecture of nodding duck wave power generators". *The Naval Architect*, Jan., pp. 21–24.

[4] Salter, S., 2016. "Wave energy: Nostalgic Ramblings, future hopes and heretical suggestions". *Journal of Ocean Engineering and Marine Energy,* ***2***(4), Nov., pp. 399–428.

[5] Whittaker, T., and Folley, M., 2012. "Nearshore oscillating wave surge converters and the development of Oyster". *Philosophical Transactions of the Royal Society A: Mathematical, Physical and Engineering Sciences*, Jan. Publisher: The Royal Society Publishing.

[6] Falcão, A. F. O., Cândido, J. J., Justino, P. A. P., and Henriques, J. C. C., 2012. "Hydrodynamics of the IPS buoy wave energy converter including the effect of non-uniform acceleration tube cross section". *Renewable Energy,* ***41***, May, pp. 105–114.

[7] Parkin, P., Payne, G., and Taylor, J., 2003. "Numerical simulation and tank tests of the free floating sloped IPS buoy". *Fifth European Wave Energy Conference. University College Cork, 17020th september*.

[8] Newman, J. N., 1977. *Marine hydrodynamics*. MIT Press, Cambridge, Mass.

[9] Falnes, J., 2002. *Ocean Waves and Oscillating Systems: Linear Interactions Including Wave-Energy Extraction*. Cambridge University Press, Cambridge.

[10] Falnes, J., and Kurniawan, A., 2015. "Fundamental formulae for wave-energy conversion". *Royal Society Open Science,* ***2***(3), Mar., p. 140305.

[11] Yu, Y.-H., Li, Y., Hallett, K., and Hotimsky, C., 2014. "Design and Analysis for a Floating Oscillating Surge Wave Energy Converter". In Volume 9B: Ocean Renewable Energy, American Society of Mechanical Engineers, p. V09BT09A048.

[12] Li, Y., and Yu, Y.-H., 2012. "A synthesis of numerical methods for modeling wave energy converter-point absorbers". *Renewable and Sustainable Energy Reviews,* ***16***(6), Aug., pp. 4352–4364. Number: 6.

[13] Le Méhauté, B., 1976. *An introduction to hydrodynamics and water waves*. New York : Springer-Verlag.

[14] Wei, Y., Rafiee, A., Henry, A., and Dias, F., 2015. "Wave interaction with an oscillating wave surge converter, Part I: Viscous effects". *Ocean Engineering,* ***104***, pp. 185–203.

[15] Wei, Y., Abadie, T., Henry, A., and Dias, F., 2016. "Wave interaction with an Oscillating Wave Surge Converter. Part II: Slamming". *Ocean Engineering,* ***113***, Feb., pp. 319–334.

[16] Ruehl, K., Ogden, D., Yu, Y.-H., Keester, A., Tom, N., Forbush, D., and Leon, J., 2021. WEC-Sim v4.4, Oct.

[17] Kurniawan, A., and Moan, T., 2012. "Characteristics of a Pitching Wave Absorber with Rotatable flap". *Energy Procedia,* ***20***, pp. 134–147.

[18] Renzi, E., and Dias, F., 2013. "Hydrodynamics of the oscillating wave surge converter in the open ocean". *European Journal of Mechanics - B/Fluids,* ***41***, Sept., pp. 1–10.

[19] Choiniere, M., Tom, N., and Thiagarajan, K., 2019. "Load shedding characteristics of an oscillating surge wave energy converter with variable geometry". *Ocean Engineering*.

[20] Henry, A., Rafiee, A., Schmitt, P., Dias, F., and Whittaker, T., 2014. "The characteristics of wave impacts on an oscillating wave surge converter". *Journal of Ocean and Wind Energy,*

1(2), pp. 101–110.

[21] Renzi, E., and Dias, F., 2012. "Resonant behaviour of an oscillating wave energy converter in a channel". *Journal of Fluid Mechanics,* ***701***, June, pp. 482–510. Publisher: Cambridge University Press.

[22] Renzi, E., and Dias, F., 2013. "Relations for a periodic array of flap-type wave energy converters". *Applied Ocean Research,* ***39***, Jan., pp. 31–39.

[23] Renzi, E., Doherty, K., Henry, A., and Dias, F., 2014. "How does Oyster work? The simple interpretation of Oyster mathematics". *European Journal of Mechanics - B/Fluids,* ***47***, Sept., pp. 124–131.

[24] Ogden, D., Ruehl, K., Yu, Y.-H., Keester, A., Forbush, D., Leon, J., and Tom, N., 2021. "Review of WEC-Sim Development and Applications". In Proceedings of the 14th European Wave and Tidal Energy Conference (EWTEC 2021), Plymouth, UK, pp. 5–9.

[25] Tom, N., Lawson, M., Yu, Y.-H., and Wright, A., 2015. "Preliminary Analysis of an Oscillating Surge Wave Energy Converter with Controlled Geometry: Preprint". p. 12.

[26] Tom, N. M., Lawson, M. J., Yu, Y. H., and Wright, A. D., 2016. "Development of a nearshore oscillating surge wave energy converter with variable geometry". *Renewable Energy,* ***96***, Oct., pp. 410–424.

[27] Tom, N., Lawson, M., Yu, Y.-H., and Wright, A., 2016. "Spectral modeling of an oscillating surge wave energy converter with control surfaces". *Applied Ocean Research,* ***56***, pp. 143–156.

[28] Tom, N. M., Yu, Y. H., Wright, A. D., and Lawson, M. J., 2017. "Pseudo-spectral control of a novel oscillating surge wave energy converter in regular waves for power optimization including load reduction". *Ocean Engineering,* ***137***, pp. 352–366.

[29] Henry, A., 2009. "The Hydrodynamics of small seabed mounted bottom hinged wave energy converters in shallow water". PhD thesis, Jan.

[30] Kelly, M., Tom, N., Yu, Y.-H., Wright, A., and Lawson, M., 2020. "Annual Performance of the Second-Generation Variable-Geometry Oscillating Surge Wave Energy Converter". *Renewable Energy*, Nov.

[31] Burge, C., Tom, N., Thiagarajan, K., Davis, J., and Nguyen, N., 2021. "Performance Modeling of a Variable-Geometry Oscillating Surge Wave Energy Converter on a Raised Foundation". In International Conference on Offshore Mechanics and Arctic Engineering, Vol. 85192, American Society of Mechanical Engineers, p. V009T09A010.

[32] US Department of Energy Office Of Energy Efficiency & Renewable Energy, . Technology Commercialization Fund.

[33] Nugyen, N., Davis, J., Thiagarajan, K., Tom, N., and Burge, C., 2021. Optimizing Power Generation of a Bottom-Raised Oscillating Surge Wave Energy Converter Using a Theoretical Model. Tech. rep., National Renewable Energy Lab.(NREL), Golden, CO (United States).

[34] Cummins, W., 1962. "The Impulse Response Function and Ship Motion". *Report 1661, Department of the Navy, David W. Taylor Model Basin, Hydromechanics Laboratory, Research and Development Report, October 1962*.

[35] Mei, C., 1989. *The Applied Dynamics of Ocean Surface Waves*. Advanced series on ocean engineering. World Scientific.